EUROPEAN FUSION DEVELOPMENT AGREEMENT

EFDA–JET–CP(04)07-17

I.H.Hutchinson, S.M.Wolfe, R.S.Granetz, J.E.Rice, A.E.Hubbard, J.Irby,
R.J.Buttery, T.C.Hender, D.F.Howell and JET EFDA Contributors

Asymmetric-Field Mode Locking in Alcator C-Mod

Asymmetric-Field Mode Locking in Alcator C-Mod

I.H. Hutchinson[1], S.M. Wolfe[1], R.S. Granetz[1], J.E. Rice[1], A.E. Hubbard[1], J. Irby[1], R.J. Buttery[2], T.C. Hender[2], D.F. Howell[2] and JET EFDA Contributors*

[1]Plasma Science and Fusion Center, MIT, Cambridge, MA, USA
[2]EURATOM/UKAEA Fusion Association, Culham Science Centre, Abingdon, OX14 3DB, UK
** See annex of J. Pamela et al, "Overview of JET Results ",*
(Proc.20 [th] IAEA Fusion Energy Conference, Vilamoura, Portugal (2004).

Preprint of Paper to be submitted for publication in Proceedings of the
20th IAEA Conference,
(Vilamoura, Portugal 1-6 November 2004)

“This document is intended for publication in the open literature. It is made available on the understanding that it may not be further circulated and extracts or references may not be published prior to publication of the original when applicable, or without the consent of the Publications Officer, EFDA, Culham Science Centre, Abingdon, Oxon, OX14 3DB, UK.”

“Enquiries about Copyright and reproduction should be addressed to the Publications Officer, EFDA, Culham Science Centre, Abingdon, Oxon, OX14 3DB, UK.”

ABSTRACT

Asymmetric field coils have been installed on Alcator C-Mod and used to establish the locked mode threshold and scaling for this compact size device. The magnitude and phase of the intrinsic field error has been identified and is found to be consistent with a comprehensive model of the sources of field errors. There proves to be no major difference between the fractional (m = 2, n = 1) field level (typically 10^{-4} of toroidal field) for mode locking on Alcator and that on JET (which has 4.3 times the linear dimensions) for typical densities on each machine. The results are consistent with a linear scaling of the total asymmetric field locking threshold with density, as has been observed elsewhere, are within a factor of 2 of the scaling previously deduced from the toroidal field scaling on JET or DIII-D using Connor-Taylor constraints, and agree with specific dimensionless identity experiments on JET.

1. INTRODUCTION AND COIL DESCRIPTION

Even very small asymmetric fields in tokamaks are important in their influence upon plasma rotation, and can give rise to major confinement perturbations in the form of "locked modes" even at low pressure. Concern has previously arisen that for ITER the allowable level of non-axisymmetry may be extremely small and diffcult to achieve. Empirical size-scaling observations [1] initially suggested a strongly unfavorable scaling to large devices. Subsequent arguments based on dimensional similarity and similarity experiments give a more optimistic extrapolation [2], but the present work provides the first experimental confirmation based on observations over a wide spread of tokamak sizes of this more optimistic view.

Asymmetric field coils have been installed on Alcator C-Mod [3] and used to establish the locked mode threshold and scaling for this compact size (R = 0.67m, a = 0.21m), highmagnetic field device. The plasma linear dimensions are thus about 1/9 that of ITER, while the typical operating field of 5.3 T, and operation up to 8 T, is approximately the same. The typical range of density in C-Mod is $2 \times 10^{19} \leq \bar{n}_e \leq 10^{21} m^{-3}$; plasma currents up to 2MA have been explored.

The new coil set refered to as the "A-coils", was installed in 2003. It serves both as an error suppressor and as a tool for investigating the physics of locked modes. The A-coils, shown schematically in figure 1, are wound from 4/0 welding cable enclosed in aluminum coil-cases and mounted on the outside of the concrete radiation shield ("igloo") which surrounds the tokamak. The full coil set consists of eight coils (only seven were installed for the experiments reported here) consisting of 27 turns each in a racetrack shape. These coils can be connected in series or parallel in a variety of configurations, allowing a range of phase and helicity as well as different poloidal mode spectra. The maximum current available from the single power supply used for these experiments was 3700A, which limits the applied m = 2 component to a maximum of about 1.2mT at the q = 2 surface.

Examples of accessible mode structures, evaluated at the q = 2 surface for a typical C-Mod equilibrium, are shown in Figure 2 for several coil combinations. Here the helical Fourier components

in straight field line geometry are defined as

$$B_{mn} = \frac{1}{2\pi^2} \int_0^{2\pi} \delta\phi \int_0^{2\pi} d\hat{\theta}\, B_\perp(\phi, \hat{\theta})\, e^{-j(n\phi + m\hat{\theta})} \tag{1}$$

where $B_\perp$ is the field normal to the rational surface and the poloidal angle is given by

$$\theta = \frac{1}{q} \oint dl \frac{B_\phi}{R B_p} \tag{2}$$

with $\hat{\theta} = 0$ corresponding to the outboard, i.e. low-field side, midplane.

The sign convention is chosen such that positive m/n correspond to the resonant helicity for C-Mod discharges with I || B. As seen in the figure, the field produced by the A-coil is dominantly in the low mnumbers, *m* = 1, 2, with a smaller contribution at *m* = 3. This is because the machine construction mandated their being placed rather far from the plasma, as shown in fig.1. Nevertheless, the ratio of *m* = 1 to *m* = 2 can be varied over a factor of five by suitable choice of coil connections.

2. LOCKING AND ERROR COMPENSATION

In C-Mod the appearance of locked modes is not always obvious on magnetic signals. However, there is very frequently a very clear influence on the size and frequency of sawteeth, which we attribute to changes in temperature and current density profile caused by the magnetic islands. Moreover, in C-Mod locking leads to a clear halting of the plasma rotation even in ohmic plasmas such as is shown in figure 3. The velocity shown is that of the plasma center, showing both that the braking effect has halted the entire core, and that there is negligible difference between the “natural” frequency of mode rotation (which is what is theoretically thought to be brought to zero) and the ion velocity, at least in the locked state.

Different coil configurations have been used to identify the magnitude and phase of the intrinsic field error, by nulling out the total asymmetry. Figure 4 summarizes a comprehensive example at B_t = 4T, I_p = 0.6MA.

The locked region is delineated by the numbered blue lines, each of which indicates the applied B_{21} evolution during a different plasma when a locked mode exists. Auxiliary experiments verify that the rest of the second and fourth quadrants are locked regions, leaving an approximately circular region in which locking does not occur. This is interpreted as centered on a value which best compensates the instrinsic field, and having a radius equal to the locked mode penetration threshold for this plasma. We deduce here $-B_{instrinsic} \approx 0.25+0.25i$ mT and $B_{lock} \approx 0.35$mT at this density ($\sim 5\times10^{19}\mathrm{m}^{-3}$).

This illustrates the result that fractional field thresholds (typically $B_{21} \sim 10^{-4}B_T$) for mode locking on Alcator are similar to those on other large tokamaks, for example JET (which has 4.3 times the linear dimensions) for typical densities on each machine.

The extent to which the intrinsic error field has been identified and corrected can be judged in

part by how low a density can then be achieved without the appearance of a locked mode.

In figure 5. we show an example of three plasmas with different density evolutions but otherwise similar parameters. In the high density case (green), an adverse asymmetric field was applied, leading to a locked mode at $n_e = 1.7\times10^{20}\mathrm{m}^{-3}$. The intermediate density case (purple) locks with zero applied field at $n_e = 1.1\times10^{20}\mathrm{m}^{-3}$. The lateness of the appearance of the mode in these two cases shows that they are close to threshold. The intrinsic error increases with time till threshold is reached. The low density case (black) has an approximately optimum correction field applied. It shows no locked mode even though its density falls to $n_e = 0.4\times10^{20}\mathrm{m}^{-3}$, four times lower than the high density case. This factor 4 density reduction shows that the intrinsic error is rather well compensated.

The results of a density scaling experiment on C-Mod at B_t = 5.4T, I_p = 1MA, and q_{95} = 3.9, are shown in figure 6. The asymmetric applied field in this case is phased to align with the intrinsic field and a series of different density and applied field shots are plotted showing those that do (crosses) or do not (diamonds) produce locking.

The results are consistent with a linear scaling of the total asymmetric field locking threshold with density, as has been observed elsewhere. This would correspond to a V-shaped boundary; our best fit is indicated and indicates an intrinsic error (the lower point of the V) of approximately 0.6 mT for these conditions. The bottom of the V contains locked points which can be explained by incomplete field compensation because of phase mismatch or side-band effects (i.e. the influence of m = 1, 3... field components).

The prior scaling [2] took the locking field to depend on density and field, and derived from the fits to those dependencies a form $B_{lock}/B_T \propto n^{\alpha n} B^{\alpha B} R^{2\alpha n+1.25\alpha B}$ based on dimensionless similarity. The predictions of the resulting scaling laws, based on fits of density and BT scalings on JET and DIIID separately, are shown in figure 6. The scalings attempted to account for side-band effects and incorporate them using coefficients that were ex-perimentally fitted. We do not have independent experimental evidence for appropriate side-band coefficients in C-Mod; therefore we plot the scalings both ignoring side-bands and using the prior side-band coefficients with the calculated applied-field side-band amplitudes. The C-Mod results are approximately a factor of two higher in density ignoring side-bands. Including side-bands reduces the discrepancy; but it still appears C-Mod locks perhaps somewhat more easily than the scaling would imply for this plasma. However, we note that since the C-Mod instrinsic-error-field side-bands are uncertain, they have been ignored here.

3. INTRINSIC FIELD ERROR

It was impractical to perform specific high-precision measurements of the intrinsic field errors, because the plasma coil-configuration requires operation at cryogenic temperatures, and hence the machine to be under vacuum. Therefore a thorough survey of identifiable design and construction field errors was performed, followed by careful measurements with existing magnetic diagnostics and a detailed fitting procedure.

Several design contributions to the error fields from non-axisymmetric currents were identified. The most significant were from the toroidal field bus and the layer-tolayer transitions in the central OH solenoid illustrated in figure 7.

The calculated “as-built” nonaxisymmetric mode amplitudes due to the TF bus and OH windings are shown in figure 8 for typical currents in these coils. The toroidal phase of the calculated $m = 2$, $n = 1$ components due to these known asymmetries is consistent with the inferred experimental error fields but alone is insufficient to explain them.

Undocumented non-axisymmetric error fields can also arise from positioning or manufacturing errors in the poloidal field coil system. The design positioning tolerance for these coils is of the order of mm, but no as-built survey of the actual locations at this scale of accuracy is available. We have therefore attempted to estimate the deviations of these coils based on *in situ* magnetic measurements.

We model the non-axisymmetric positioning errors of each of the principal components of the PF system as a combination of rigid n = 1 Tilts (T) and Horizontal shifts (H).

An experiment was carried out, without plasma, energizing individual PF coils, using currents typical of those encountered during plasma operation, and pulse lengths of 1–2 seconds to allow for evaluation of field penetration effects. The basic measurements for the analysis consist of the *difference signals* of pairs of field measurement coils at the same poloidal locations but different toroidal angle, corrected for “known” design asymmetries, as discussed above

$$\breve{} _{ij} \equiv (B_j - B_i) - \breve{} _{ij}^{\,DESIGN} . \qquad (3)$$

The observed difference signals Δij are of the order of 10^{-3} of the absolute signal levels $B_i \approx B_j$, which is substantially smaller than the nominal calibration errors. Therefore the position (R, Z), orientation (θ), and calibration (G) of the sensors was included in the fitting procedure. Schematically, then, we solve

$$\sigma_{\breve{}}^{-1} \begin{Bmatrix} \breve{}_{ij}^{(1)} \\ \breve{}_{ij}^{(2)} \\ \vdots \\ \breve{}_{ij}^{(N)} \end{Bmatrix} = \left(\sigma_{\breve{}}^{-1} \begin{bmatrix} \frac{\partial \breve{}_{ij}^{(1)}}{\partial H^{(p)}} & \frac{\partial \breve{}_{ij}^{(1)}}{\partial T^{(p)}} & B_i^{(1)} & \frac{\partial B_i^{(1)}}{\partial R_i} & \frac{\partial B_i^{(1)}}{\partial Z_i} & \frac{\partial B_i^{(1)}}{\partial \phi_i} \\ \frac{\partial \breve{}_{ij}^{(2)}}{\partial H^{(p)}} & \frac{\partial \breve{}_{ij}^{(2)}}{\partial T^{(p)}} & B_i^{(2)} & \frac{\partial B_i^{(2)}}{\partial R_i} & \frac{\partial B_i^{(2)}}{\partial Z_i} & \frac{\partial B_i^{(2)}}{\partial \phi_i} \\ \vdots & & \vdots & & \vdots & \\ \frac{\partial \breve{}_{ij}^{(N)}}{\partial H^{(p)}} & \frac{\partial \breve{}_{ij}^{(N)}}{\partial T^{(p)}} & B_i^{(N)} & \frac{\partial B_i^{(N)}}{\partial R_i} & \frac{\partial B_i^{(N)}}{\partial Z_i} & \frac{\partial B_i^{(N)}}{\partial \phi_i} \end{bmatrix} \sigma_x \right) \sigma_x^{-1} \begin{Bmatrix} H^{(p)} \\ T^{(p)} \\ \zeta G_{ij} \\ \delta R_{ij} \\ \delta Z_{ij} \\ \delta \theta_{ij} \end{Bmatrix} \qquad (4)$$

in a least-squares sense, by singular value decomposition. We use independent heuristic uncertainty (σ) estimates, and retain 240 of 248 principal vectors giving a reduced χ^2 of approximately one.

The results for the tilts and shifts, shown in figure 9, are plausible considering assembly tolerances, showing displacements of the order of a few millimeters. However, this model cannot account for any asymmetries in the TF magnet itself; we have no capability of measuring such effects with presently installed diagnostics since they cannot be distinguished from a tilt of the measurement

coil in the toroidal direction. For typical discharges, the fitted tilts and shifts correspond to non-axisymmetric field pertubations of a few times 10^{-4} tesla.

When combined with the calculated contributions from the "as-built" non-axisymmetric fields the total instrinsic error deduced appears consistent in magnitude and orientation, with the results of locked mode experiments using the A-coils. Figure 10 shows an example. The solid lines show a locked mode which occurs without applied B_{21} field. It is caused by the intrinsic fields whose components are reconstructed as a function of time. The swing of the ohmic transformer causes the error to increase as a function of time, thus explaining the observed delay of locking. With applied field, the total (2,1) error amplitude is reduced by a factor of about 4 and no locking occurs.

4. DIMENSIONLESS IDENTITY JET COMPARISON

To establish more thoroughly the scaling of the locking threshold, a specific experiment has been performed to compare results from JET and C-Mod in closely similar configurations. This called for operation of C-Mod at B_t = 6.3T, I_p = 1.3MA, with the shapes of the plasma the same in both machines (which means at the lower/upper end of the normal triangularity for C-Mod/JET respectively: ~0.43 at the x-point). JET parameters were B_t = 0.98T, I_p = 0.88MA, and the heating was purely ohmic, so that the plasmas were as far as possible dimensionlessly identical according to Connor- Taylor constraints ($n_e a^2$ and $Ba^{4/5}$ constant). Density and temperature profiles, when scaled accordingly, were observed to agree well. A very wide density range (> factor of 4) was investigated.

The C-Mod coil configuration (Bt,-Db,-Gt,Jb) was chosen specifically to match as closely as possible the sideband spectrum of the JET Error Field Correction Coils. This configuration has nominal (m = 2) phase -0.31 radians, which is substantially different from the intrinsic error field, which figure 4 indicates is -2.4 radians (for that lower current plasma). Therefore we expect the locking region to have a hyperbolic shape on the plane of density versus applied field.

In figure 11 we show the experimental results. There is some intermingling of locked and unlocked plasmas, which we attribute to hidden variability. Because of this, we show two extreme hyperbolic fits corresponding to n_e/B^{tot} = 2.7 (dashed curve) and 4.0 (chain curve) times 10^{23} m^{-3}/T. Both fitted intrinsic error (m = 2) phases are close to -3 radians. The presence of the intrinsic error compromises the error-field $_{21}$ spectrum match to some extent, since the intrinsic sideband spectrum is uncontrolled.

Using the C-Mod model of instrinsic field discussed in the previous section, we can perform a broader comparison, including additional data from two other A-coil configurations with phase angles of –0.7 and 1.9 radians respectively, and converting to total B_{21} amplitude using the modelled rather than fitted intrinsic field. Figure 12 shows a gratifying convergence of the results. The agreement between C-Mod and the scaled JET results is clearly well within the experimental uncertainty, consistent with dimensionless identity.

CONCLUSION

In summary, Alcator CMod results directly confirm that axisymmetric mode locking thresholds scale moderately weakly with machine size. The scalings predict error field thresholds for ITER that will be well within the capability of the planned error correction system.

This work was supported by USDOE Grant DE-FC02-99ER54512 and partly performed under the European Fusion Development Agreement.

REFERENCES

[1]. R.LaHayGeneralAtomics Report GA-A22468 (1997).

[2]. R.Buttery et al, Nuclear Fusion **39**, 1827 (1999).

[3]. R.Vieira et al, Proceedings of the 20th IEEE/NPSS Symposium on Fusion Engineering 2003, IEEE, to be published.

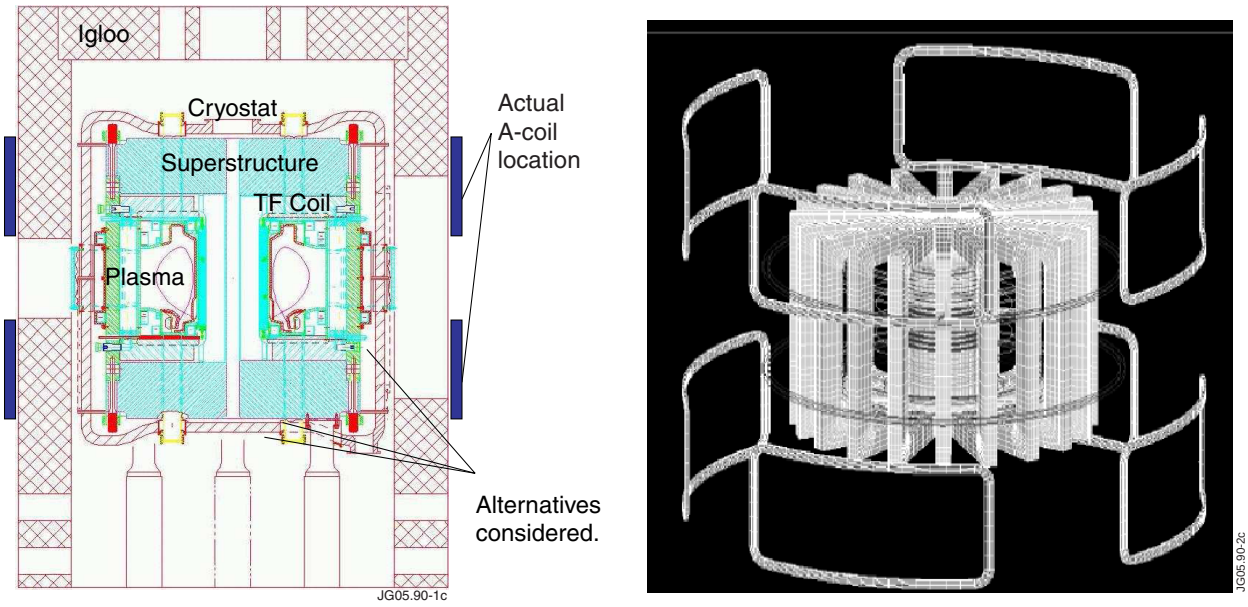

Figure 1: Non-axisymmetric field coils (A-coils) are mounted to the concrete igloo surrounding the tokamak. Pairs of coils are located above and below the midplane at four toroidal locations.

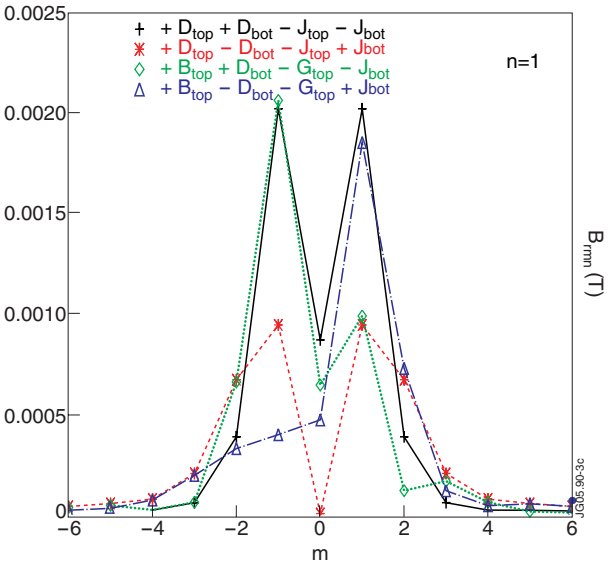

Figure 2: Calculated poloidal mode amplitudes for n = 1 with different combinations of four A-coils in series, at A-coil current of 2.3kA.

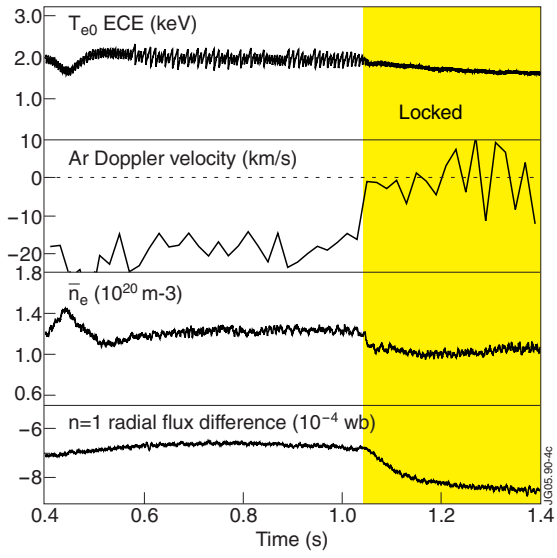

Figure 3: Mode locking due to intrinsic field error, showing the effect on sawteeth in the central temperature, rapid elimination of the (negative) plasma rotation, density reduction, and signal on locked-mode-sensitive flux loops.

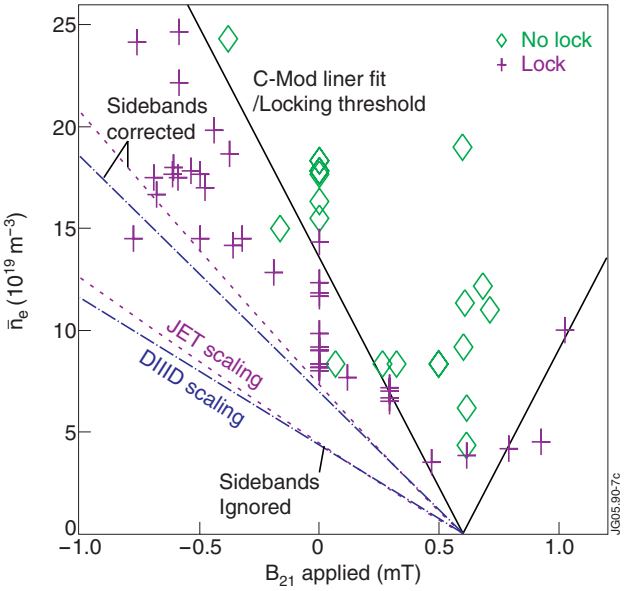

Figure 6: Scaling of C-Mod mode locking results compared with the prior scalings from JET and DIIID.

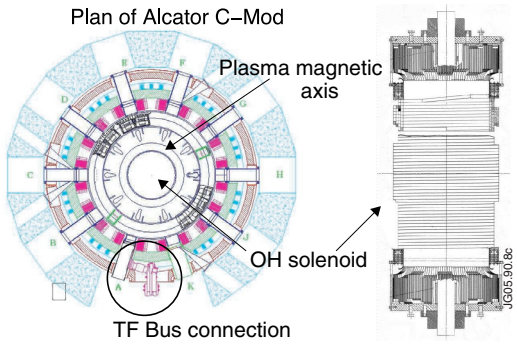

Figure 7: Right: Plan showing TF connections. Left: OH winding section

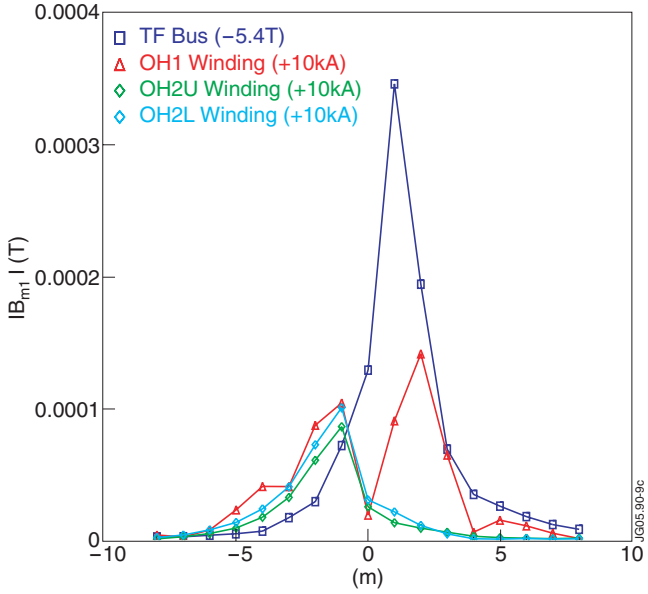

Figure 8. Calculated (n=1) mode amplitudes for versus poloidal mode number, m, from typical currents in the TF bus and OH coil windings

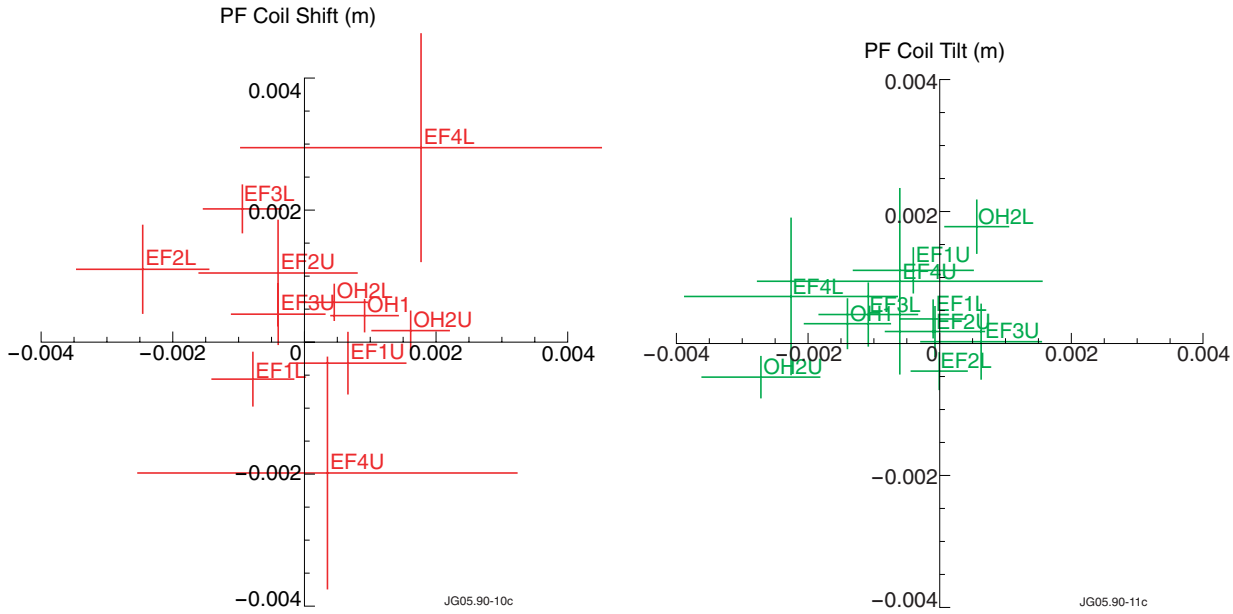

Figure 9: PF coil shifts and tilts inferred from regression analysis

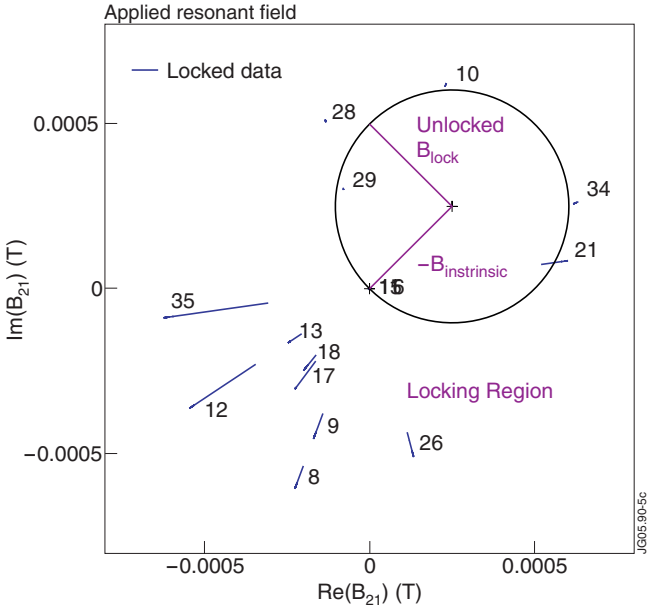

Figure 4: Complex amplitude plane of applied (2,1) field showing regions of locked and unlocked behavior.

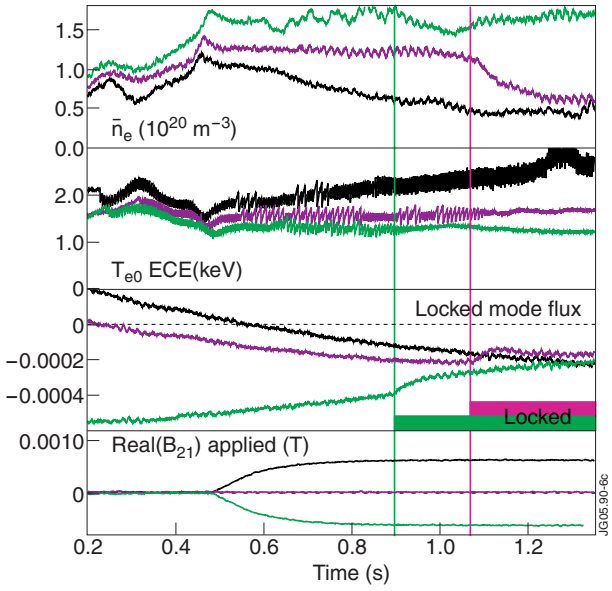

Figure 5: Evolution of different density plasmas shows correction permits operation down to very low density.

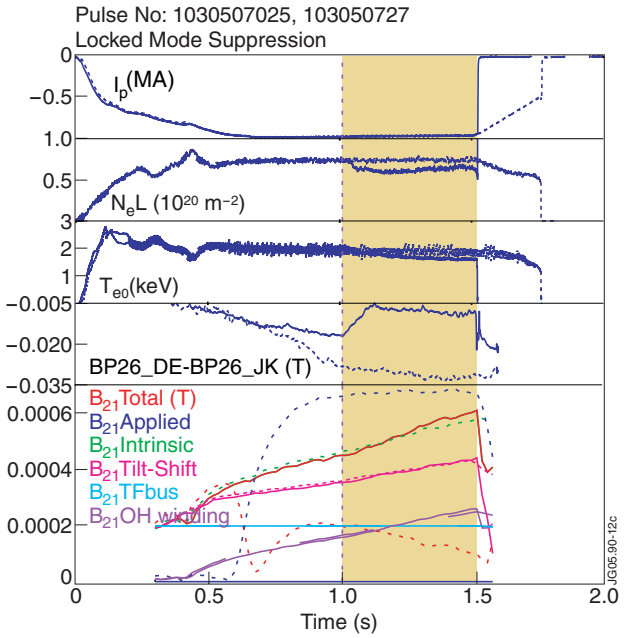

Figure 10: Example of reconstructed error field versus time (in seconds) without (solid) and with (dashed) applied non-axisymmetric field.

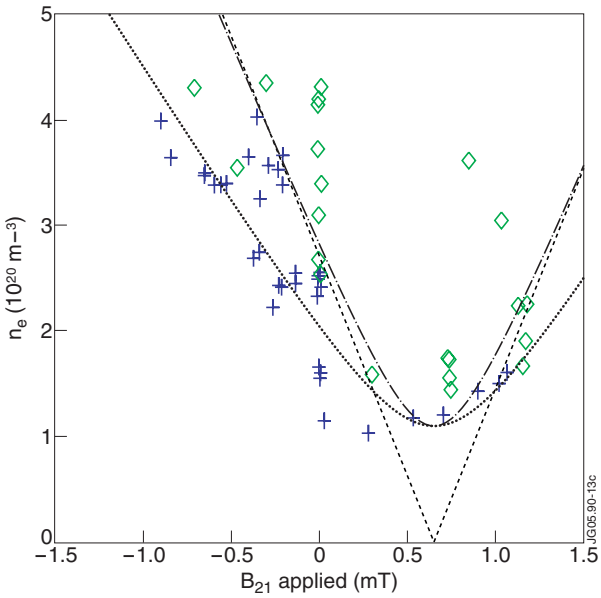

Figure 11: C-mod Locking region for the JET/C-mod similar plasmas. Crosses denoted locked plasmas, diamonds unlocked.

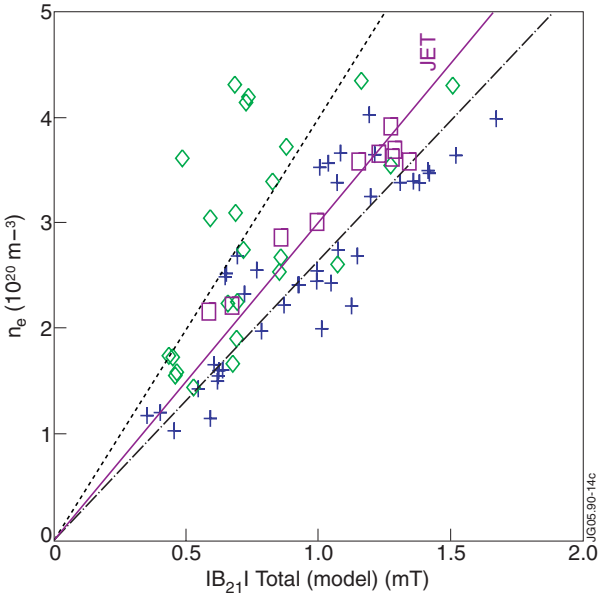

Figure 12: Dimensionally scaled JET locking threshold (squares) compared with C-mod locked (crosses) and unlocked (diamonds) data.